

HEAT TRANSFER IN A TURBULENT CHANNEL FLOW WITH SUPER-HYDROPHOBIC OR LIQUID-INFUSED SURFACES ON ONE WALL

Umberto Ciri

Department of Mechanical Engineering
The University of Texas at Dallas
800 W Campbell Rd, Richardson, TX 75252 US
umberto.ciri@utdallas.edu

Stefano Leonardi

Department of Mechanical Engineering
The University of Texas at Dallas
800 W Campbell Rd, Richardson, TX 75252 US
stefano.leonardi@utdallas.edu

ABSTRACT

The thermal performance of super-hydrophobic and liquid infused surfaces (SHS and LIS, respectively) in turbulent flows is investigated using direct numerical simulations. These surfaces consist of a micro-texture (typically ridges or posts) with cavities filled with a secondary fluid which generates a slippery interface with the primary fluid (typically water). The heterogeneous solid-fluid and fluid-fluid interface created by the cavities and the secondary fluid leads to an average slip boundary, which reduces the mean shear (thus, the drag) in the overlying flow. Direct numerical simulations of turbulent flow and heat transfer are performed for a channel with a textured wall, considering different texture geometries and viscosity ratios between the two fluids. We first assume that the interface between the two fluids remains flat, representing the asymptotic case of infinite surface tension (equivalently, Weber number $We = 0$). Results indicate that also heat transfer efficiency may be increased compared to the smooth wall thanks to the strong drag reduction, although the surface heat flux is reduced. A second set of simulations with deformable interface has been performed, assuming a Weber number $We = 40$ ($We^+ = 10^{-3}$), which implies a finite surface tension. In this latter case, the heat transfer efficiency remains larger than the smooth wall reference, and for some geometries it is observed a simultaneous increase in surface heat flux and decrease in drag.

INTRODUCTION

The transport of heat and momentum in turbulent flows is an essential aspect of several engineering applications. For example, turbulent mixing is exploited for cooling gas turbine blades in engines. Turbulators or roughness elements are used in the internal passages of the blades to increase turbulence intensity and improve cooling efficiency (Han, Dutta & Ekkad, 2000; Sewall *et al.*, 2006). However, this enhancement is generally accompanied by an

increase in flow resistance or pressure drop (Leonardi *et al.*, 2015). In fact, when momentum transfer is prominent, engineers typically seek to reduce turbulence intensity so as to decrease drag, for instance in marine or aerial vehicles.

Recently, bio-inspired surface treatments such as super-hydrophobic coating or liquid-infused textures have attracted attention for potential drag reduction in turbulent flows. These surfaces are made of a micro-texture (typically ridges or posts) with cavities where a second fluid is locked and generates a slippery interface with the primary fluid. In the case of super-hydrophobic surfaces (SHS), the fluid trapped in the cavities is air, while for liquid-infused surfaces (LIS) the substrate is impregnated with a liquid lubricant immiscible with the primary fluid. The heterogeneous solid-fluid and fluid-fluid interface created by the cavities and the secondary fluid leads to an average slip boundary, which reduces the mean shear (thus, the drag) in the overlying flow. Experimental and numerical studies have corroborated this potential for drag reduction and the underlying mechanisms (Daniello, Waterhouse & Rothstein, 2009; Rosenberg *et al.*, 2016; Martell, Perot & Rothstein, 2009; Park, Park & Kim, 2013; Fu *et al.*, 2017; Arenas *et al.*, 2019).

Despite the progress made in understanding the mechanism leading to drag reduction, less is known on the heat transfer process over SHS and LIS. The present paper aims at filling this gap by discussing direct numerical simulations results of turbulent flow and heat transfer over SHS and LIS. Simulations are performed for a channel with a textured wall and a second fluid inside the cavities (figure 1). Different viscosity ratios between primary and secondary fluid provide an idealised representation of either LIS or SHS, while thermal properties are assumed to be uniform across the channel and the Prandtl number unitary. The aim of the work is to investigate the contribution of the turbulent motion to the heat transfer. We assess the dependence on the substrate geometry considering longitudinal and transversal textures and conducting a parametric study

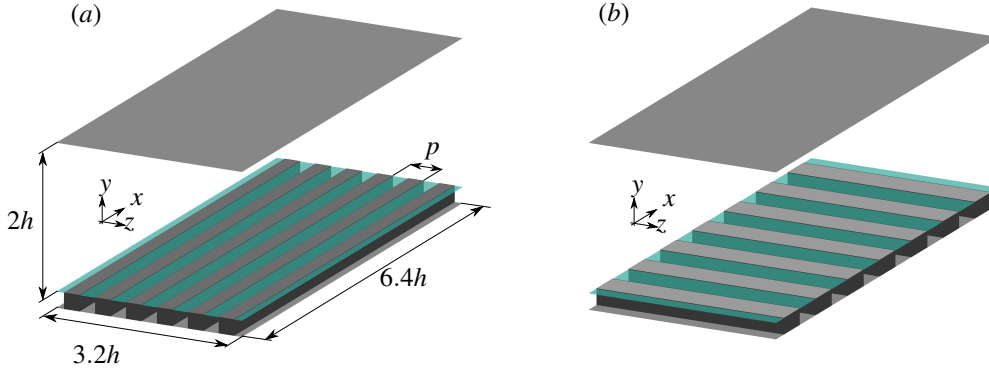


Figure 1. Configuration of the channel flow (flow in the x direction): (a) longitudinal bars; (b) transversal bars. The turquoise surface at the crest plane represents the interface. Dimensions are not to scale for presentation purposes.

on the pitch-to-height ratio of the bars. We investigate the effect of the surface tension between the fluids considering two sets of simulations. In the first case, the interface is slippery but forced to remain flat, representing the asymptotic case of infinite surface tension and a Weber number $We = \rho U_b^2 h / \sigma = 0$ (here σ is the surface tension, ρ the density of the primary fluid, U_b the bulk velocity and h the half-height of the channel). Afterwards, the interface is allowed to deform based on the evolution of the flow and assuming $We = 40$, which approximately corresponds to a Capillary number $Ca = We^+ = \mu u_\tau / \sigma \sim 10^{-3}$; μ is the viscosity of the primary fluid and $u_\tau = \sqrt{\tau / \rho}$ is the friction velocity (τ is the drag per unit area of the textured wall). The surface performance, in terms of drag (τ) and heat flux (q), is compared with a channel with smooth walls and the same flow rate.

NUMERICAL METHODOLOGY

The continuity, Navier-Stokes and energy equations for two super-posed fluids are:

$$\frac{\partial U_i}{\partial x_i} = 0 \quad (1)$$

$$\frac{\partial U_i}{\partial t} + \frac{\partial U_i U_j}{\partial x_j} = -\frac{\partial P}{\partial x_i} + \Pi \delta_{i1} + \frac{1}{Re} \frac{\partial}{\partial x_j} 2\tilde{\mu} S_{ij} + f_i \quad (2)$$

$$\frac{\partial T}{\partial t} + \frac{\partial}{\partial x_j} (T U_j) = \frac{1}{Re Pr} \frac{\partial}{\partial x_j} \left[\tilde{\alpha}(\phi) \frac{\partial T}{\partial x_j} \right] \quad (3)$$

U_i is the component of the velocity vector in direction x_i , P is the pressure and T the fluid temperature. Π is the pressure gradient required to maintain a constant flow rate, S_{ij} is the symmetric part of the velocity gradient tensor and f_i is the force at the interface in direction x_i . The Reynolds number, Re , is based on the channel half-height h , the (constant) bulk velocity U_b and the viscosity of the overlying fluid ($\nu_2 = \mu_2 / \rho$). For the present simulations, $Re = U_b h / \nu_2 = 2,800$. The Prandtl number, $Pr = \nu_2 / \alpha_2 = 1$, is also defined with the properties of the fluid in the bulk channel, with α_2 being the thermal diffusivity. The marker functions $\tilde{\mu}(\phi)$ and $\tilde{\alpha}(\phi)$ discriminate between the properties of the

two fluids based on the signed distance from the interface ϕ (positive in the main fluid, negative for the secondary fluid). The marker function is defined as $\tilde{\alpha}(\phi) = a + (1 - a)H(\phi)$, where H is the Heaviside function ($H = 0$ if $\phi < 0$, secondary fluid; and $H = 1$ if $\phi > 0$, main fluid); $a = \alpha_1 / \alpha_2$ is the diffusivity ratio between the fluids and is taken as unity to isolate the effect of heat convection. $\tilde{\mu}$ is defined analogously, with the viscosity ratio m instead of a . Two viscosity ratios have been considered: $m = \mu_1 / \mu_2 = 0.01$ (SHS, water over air), and $m = 0.4$ (LIS, water over heptane).

The force at the interface f_i is given by:

$$f_i = \frac{1}{We} \kappa n_i \delta(\phi) \quad (4)$$

where δ is the Dirac delta function, n_i is the component in direction x_i of the normal to the interface, κ is the curvature of the interface. $We = \rho U_b^2 h / \sigma$ is the Weber number, with σ being the surface tension between the two fluids. We have accounted for two conditions: (i) $We = 0$, which represents the limiting case of infinite surface tension, and (ii) $We = 40$, which corresponds to a Capillary number $Ca = \mu_2 u_\tau / \sigma \sim 10^{-3}$. In the case of $We = 0$, the interface remains flat. Therefore, the force f_i in (4) is directed along the wall-normal direction (x_2 , or y), and is such that $U_2 = 0$ at the interface. The interface is slippery in the in-plane directions (x_1 and x_3). In the second case, $Ca = 10^{-3}$, the position of the interface is coupled to the Navier-Stokes equations with the level-set equation:

$$\frac{\partial \phi}{\partial t} + \frac{\partial}{\partial x_j} (U_j \phi) = 0 \quad (5)$$

The details of the numerical implementation of the level-set method can be found in García Cartagena *et al.* (2018). The numerical method for solving the fluid governing equations is described in Orlandi (2000). The substrate textures are treated with the immersed boundary method presented in detail in Orlandi & Leonardi (2006).

Simulations are performed for a turbulent channel flow with texture on the lower wall (figure 1). The surface texture consists of either longitudinal or transversal bars with (constant) height $k = 0.05h$. Three values for the pitch p between two consecutive ridges are considered, specifically $p/h = 0.1, 0.2, 0.4$. The gas fraction (i.e. the ratio of the volume of the cavities to the total volume in the substrate) is kept constant and equal to 50%. The lower wall is heated

at a constant temperature T_w . The upper, smooth, wall is kept at temperature $T_u < T_w$.

FLAT INTERFACE ($We = 0$)

The textures and the secondary fluid of LIS and SHS create a fluid-fluid interface over which the primary fluid can slip. The drag reduction of SHS and LIS is related to the slip conditions at the interface (Rastegari & Akhavan, 2015) and can be characterized by the local ‘slip length’: $\bar{U}_s = b d\bar{U}/dy$, where \bar{U}_s is the apparent ‘slip’ velocity at the crest plane and $d\bar{U}/dy$ is the local average gradient normal to the interface (Navier, 1823; Lauga & Stone, 2003). The overline denotes averages in time and in the streamwise and spanwise directions. Thus, the slip length b is the distance from the interface of the virtual no-slip boundary where the velocity profile, extrapolated with the gradient at the interface, vanishes.

Figure 2(a) shows that drag reduction ($1 - \tau/\tau_0$, where τ is the surface drag, and the subscript ‘0’ refers to the smooth wall benchmark) is well correlated with the slip length normalized in wall units ($b^+ = bu_\tau/\nu_2$). This is consistent with previous studies (Fu *et al.*, 2017; García Cartagena *et al.*, 2018) and analytical models (Rastegari & Akhavan, 2015; Fukagata *et al.*, 2006). Both LIS and SHS with transversal surface textures induce an increase in drag, and the correlation with b^+ is lost. The slip length (and hence the drag reduction or increase) is larger for SHS than LIS and increases with the pitch between the textures.

Analogously to b , a thermal slip length b_θ can be defined to link the surface gradient and the change in the average temperature at the crest plane: $T_w - \bar{T}_s = -b_\theta d\bar{T}/dy$. The thermal slip length is the distance from the interface of the virtual iso-thermal boundary at $T = T_w$. Figure 2(b) reports the percentage change in surface heat flux q (relative to the smooth wall baseline q_0) as a function of the thermal slip length b_θ^+ . The thermal slip length also increases with the pitch between the bars. Compared to the drag case, the dependence on texture orientation is opposite: transversal bars have a superior performance, although the heat flux is marginally reduced compared to the smooth wall reference. Longitudinal bars involve a more pronounced decrease in the heat transfer performance. However, the magnitude of the reduction remains limited ($< 10\%$) and is smaller than the relative reduction in drag.

For a given pitch and texture orientation, SHS and LIS have similar heat transfer performance. The dependence on the surface type is mitigated by the assumption of uniform thermal diffusivity across the two fluids ($a = 1$). The residual discrepancy, which is larger for increasing pitch (hence increasing ‘slip’ contribution), is then to ascribe to the turbulent motion over LIS and SHS.

Figure 3 shows the (non-dimensional) heat flux to drag ratio q/τ . For a smooth wall, $q/\tau = 1$ (Reynolds analogy). SHS and LIS with longitudinal ridges transfer heat more efficiently than a smooth wall, since $q/\tau > 1$. The surface heat flux is only marginally reduced compared to the decrease in skin-friction drag (figure 2). For transversal micro-textures, the efficiency factor is slightly lower than unity, similarly to classic d -type (low pitch-to-height ratio, p/k) roughness (Leonardi *et al.*, 2015). Despite the relatively large value of p/k (favorable for heat transfer enhancement, Leonardi *et al.*, 2015), the flat interface damps wall-normal fluctuations and allows the flow to skim over the crest plane. In general, wall-normal velocity fluctuations promote heat

transfer through ejections of high-temperature fluid, i.e. increasing the convective heat flux $\bar{\theta v}$ (here, $\theta = T - \bar{T}$ and $v = V - \bar{V}$). In this case, strong ejections are prevented by the interface between the two fluids. Figure 4 shows a slight increase in the heat flux in the near-wall region, particularly for transversal textures. This is due to the dispersive component induced by the solid-fluid heterogeneity at the crest plane and the consequent secondary motion. In a more realistic scenario, the interface deformation may lead also to an enhanced turbulent contribution to $\bar{\theta v}$, thus promoting heat transfer. However, larger wall-normal fluctuations increase drag (Orlandi, Leonardi & Antonia, 2006; Orlandi & Leonardi, 2008), and interface dynamics hinders drag-reducing capabilities of LIS and SHS (García Cartagena *et al.*, 2018). Therefore, the effect of the interface dynamics has been assessed by carrying out an additional set of simulations for $We = 40$ analyzed in the next section.

DYNAMIC INTERFACE

The simulations with deformable interface have been performed for the SHS textures to limit the computational costs. Figure 5(a) shows the effect of the surface tension on the drag-reduction performance. The dashed lines connects corresponding cases (geometry and pitch) for $We = 0$ (solid symbols) and $We = 40$ (empty symbols).

For longitudinal bars, the increase in Weber number leads to an increase in the streamwise slip length. Despite the increase in slip length, SHS show a considerable drop in the drag reduction performance (meaning the resistance of the surface increases). For $p/h = 0.1$, the drag becomes comparable to the smooth wall case, and for $p/h = 0.2$ the amount of drag reduction is reduced by about half. Figure 5(b) compares the mean velocity profile (\bar{U}) for longitudinal bars with $p/h = 0.2$ in the case of $We = 0$ and $We = 40$. The velocity inside the cavity ($y/h < 0$) increases considerably for $We = 40$. More momentum is transferred (and dissipated) inside the cavities by the Reynolds stresses \bar{uv} at the interface, which decreases the amount of drag reduction (Arenas *et al.*, 2019).

For the transversal obstacles, a general decrease in the slip length can be observed for the $We = 40$ cases. These surfaces remains drag-increasing and the finite surface tension tends to worsen the performance (larger drag). In general, compared to the flat interface cases, the correlation between the amount of drag reduction and the slip length becomes weaker. When the interface is forced to remain flat ($We = 0$), the wall-normal velocity fluctuations are damped and so are the Reynolds stresses \bar{uv} in the proximity of the interface. In the case of $We \neq 0$, significant Reynolds stresses can be generated at the interface, and the slip conditions (slip length and slip velocity) are no longer the only or dominant factor determining the drag, hence the decrease in the correlation (Arenas *et al.*, 2019).

Figure 6(a) shows the heat transfer enhancement as a function of the thermal slip length in wall units, b_θ^+ . For the various geometries, a decrease in the thermal slip length is observed and $b_\theta^+ \lesssim 1$. Compared to flat interface case, some textures are able to increase the heat flux respect to the smooth wall reference. In particular, super-hydrophobic longitudinal ridges simultaneously enhance heat transfer and reduce drag (Figure 5a). The deformation of the interface promotes thermal mixing through the $\bar{\theta v}$ flux, as shown in figure 6(b) for the case of SHS longitudinal bars and $p/h = 0.2$. Respect to the $We = 0$ case, the larger flux is

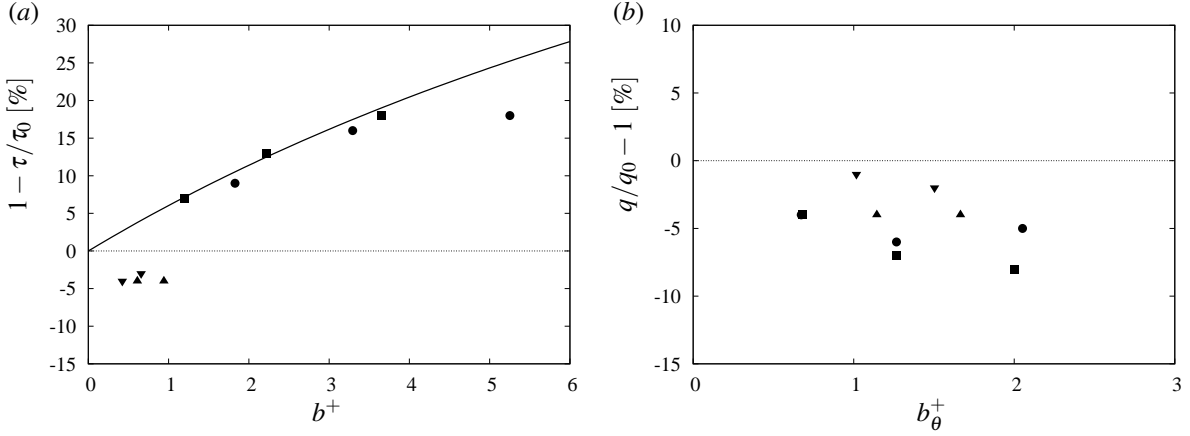


Figure 2. Overall surface performance for $We = 0$: (a) drag reduction as a function of the streamwise slip length; (b) heat transfer enhancement as a function of the thermal slip length. Longitudinal bars: SHS \bullet , LIS \blacksquare ; transversal bars: SHS \blacktriangle , LIS \blacktriangledown . The solid line in (a) shows the analytical model from Rastegari & Akhavan (2015): $(1 - \tau/\tau_0) = b^+ / (b^+ + Re/Re_\tau)$.

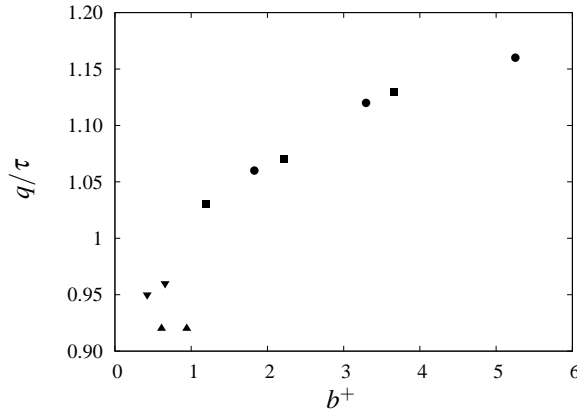


Figure 3. Non-dimensional heat-flux to drag ratio as a function of the streamwise slip length. Symbols as in Figure 2, $We = 0$.

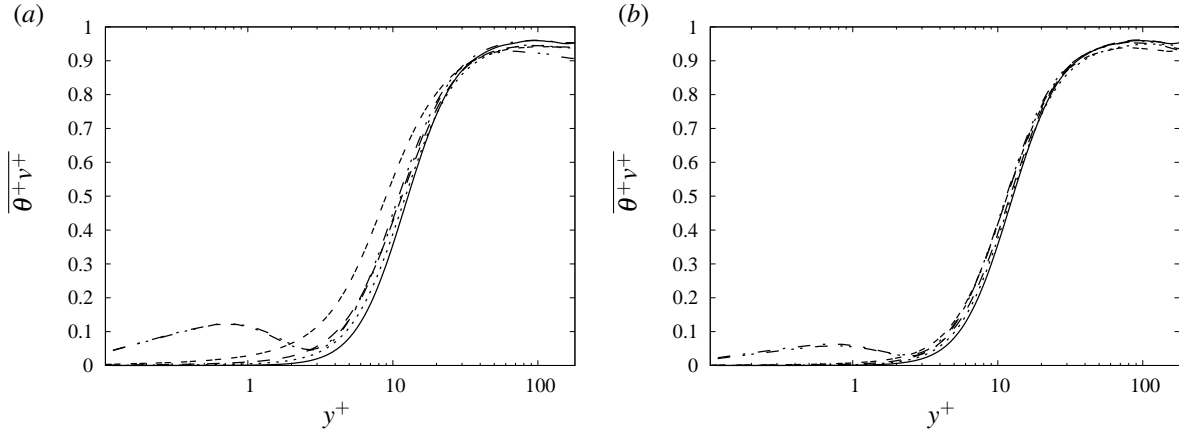


Figure 4. Convective heat flux profile ($\overline{\theta^+_{v^+}} = \overline{\theta_v \rho c_p / q}$) for SHS (a) and LIS (b): longitudinal ridges, $p/h = 0.1$; ---- longitudinal ridges, $p/h = 0.2$; - · - longitudinal ridges, $p/h = 0.4$; — transversal bars, $p/h = 0.1$; — · — transversal bars, $p/h = 0.2$. Smooth channel —.

due not only to the dispersive component of $\overline{\theta_v}$ induced by the secondary motion, but mostly to the turbulent (random) component, which increases thanks to flow ejections from the cavity. Nevertheless, the intensity of the turbulent motion at the crest is moderate because of the surface tension, which opposes transport at the interface without completely suppressing it (as in the $We = 0$ case). This is beneficial for avoiding the Reynolds stresses \overline{uv} to overcome the slip drag-

reducing mechanism, but the residual motion is enough to improve the surface heat flux.

Overall, the heat-flux to drag ratio q/τ is positively affected by the dynamics of the interface. The longitudinal geometries maintains a value above unity, which represents the smooth wall baseline, and larger than the corresponding $We = 0$ level. This is due to the increase in heat flux q caused by the interface fluctuations, which offsets the gen-

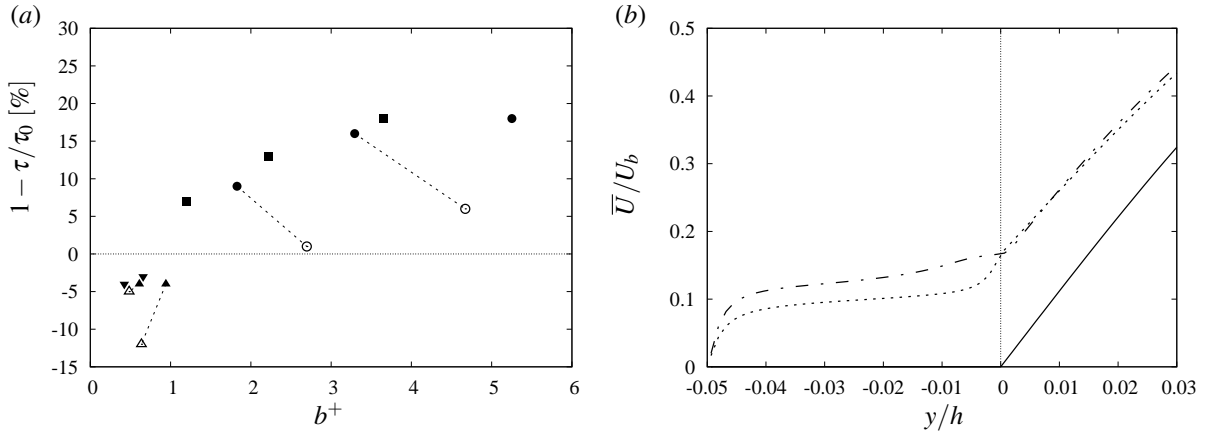


Figure 5. (a) Drag reduction as a function of the streamwise slip length: longitudinal bars: SHS \bullet , LIS \blacksquare ; transversal bars: SHS \blacktriangle , LIS \blacktriangledown . Solid symbols, $We = 0$; empty symbols, $We = 40$. (b) Mean velocity \bar{U} profile near the interface ($y/h = 0$) for SHS longitudinal ridges with $p/h = 0.2$: \cdots $We = 0$; $\dashv\dashv$ $We = 40$. Smooth channel case: — .

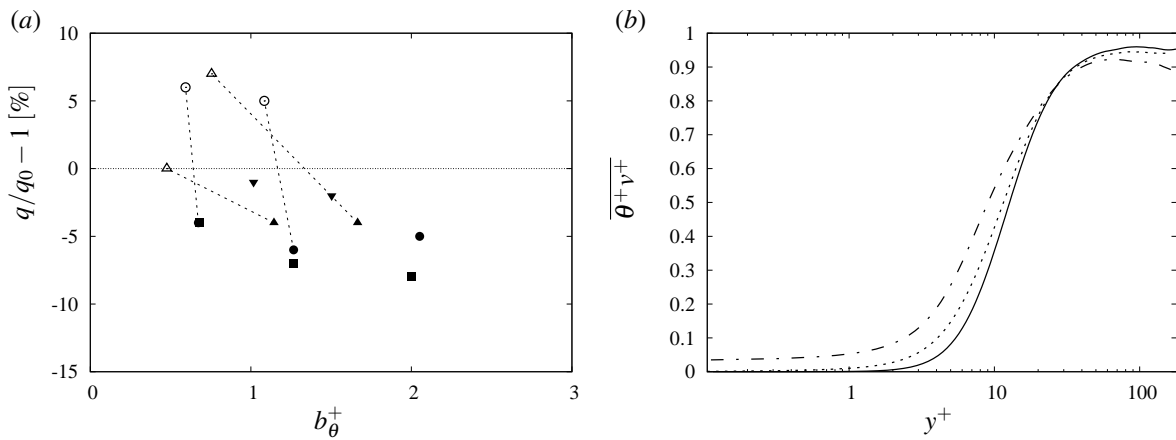


Figure 6. (a) Heat transfer enhancement as a function of the thermal slip length: longitudinal bars: SHS \bullet , LIS \blacksquare ; transversal bars: SHS \blacktriangle , LIS \blacktriangledown . Solid symbols, $We = 0$; empty symbols, $We = 40$. (b) Convective heat flux $\overline{\theta^+ \nu^+}$ for longitudinal SHS ridges with $p/h = 0.2$ as a function of the Weber number: \cdots $We = 0$; $\dashv\dashv$ $We = 40$. Smooth channel case: — .

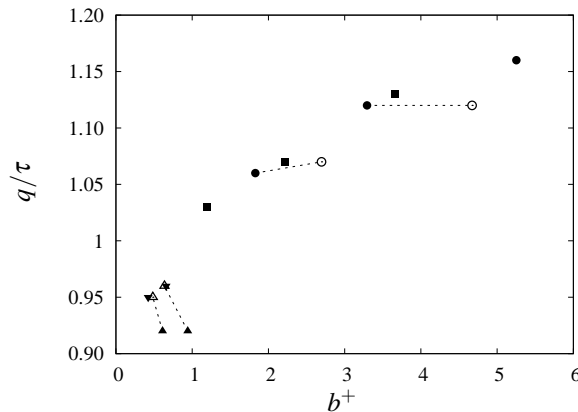


Figure 7. Non-dimensional heat-flux to drag ratio as a function of the streamwise slip length. Symbols as in Figure 6: solid, $We = 0$; empty: $We = 40$.

eral drop in drag reduction amount (figure 5a). For the case of transversal bars, the increase in We leads to an increase in the heat transfer efficiency, although the value of q/τ remains slightly smaller than the smooth channel reference. As discussed for the case of flat interface, this behavior is similar to classic transversal rough surfaces with low pitch-to-height ratio. This result suggests that, for this texture and

Weber number, the surface tension is large enough to damp most flow ejections from the cavities, which are responsible for the strong increase in heat transfer and drag of rough surfaces (Leonardi *et al.*, 2015).

CONCLUSIONS

Direct numerical simulations of turbulent heat transfer over idealised superhydrophobic and liquid infused surfaces have been performed. We have considered a channel with textures on one wall, consisting of either transversal or longitudinal bars with various pitch-to-height ratios. A secondary fluid is present in the cavities between the bars, with one viscosity ratio with the primary fluid mimicking super-hydrophobic surfaces (SHS), and another one representing liquid-infused surfaces (LIS). Two conditions are investigated for the interface between the fluids: (i) a rigid, flat interface at the crest plane, representing the asymptotic case of infinite surface tension; and (ii) deformable interface with finite surface tension (the Weber number is $We = 40$).

In the first conditions, simulations corroborate the drag-reducing capabilities of LIS and SHS observed in the literature. For longitudinal ridges, the drag can be decreased respect to the smooth wall up to 15 – 20% for LIS and SHS, with increasing drag reduction magnitude for increasing pitch between the bars. Owing to the lower viscosity of the fluid in the cavities, SHS reduce drag more than LIS for a given pitch. However, the surface heat flux is reduced respect to the smooth wall for both LIS and SHS. Transversal bars, which were found to increase drag, have better performance in this regard compared to the longitudinal ones, with a marginal decrease in the heat transfer. The rigid interface damps the velocity fluctuations close to the crest plane, thus reducing the vertical turbulent heat transport. In classic regular rough surfaces, which have an analogous configuration (textured wall, but with no interface and one fluid only), this latter is the main mechanisms by which heat transfer and drag are increased. As recently clarified by Arenas *et al.* (2019), for LIS and SHS, the presence of a rigid interface suppress this mechanism, and the opposite behavior is observed (drag reduction and decrease in heat flux). The heterogeneity at the crest plane with no-slip and slippery regions induces dispersive fluxes which mitigate these effects, in particular for transverse square bars. The heat transfer to drag ratio q/τ is found to be larger than one (which is the value for a smooth wall) for longitudinal bars, meaning that heat is transferred more efficiently despite the surface flux reduction. The texture orientation seems to have a primary effect on the heat transfer efficiency, with transversal bars presenting $q/\tau < 1$. The present results suggest a continuous transition from longitudinal SHS/LIS, $q/\tau > 1$, to smooth wall $q/\tau = 1$ and to transverse textures or classic rough surfaces, $q/\tau < 1$ (Leonardi *et al.*, 2015).

In the case of $We = 40$, the interface deformation allows the generation of wall-normal velocity fluctuations at the crest plane. This generally tends to increase the drag of the surface. More momentum is transferred and dissipated inside cavities by the Reynolds stress generated by the dynamics of the interface. The heat transfer performance is enhanced for most of the geometries compared to the $We = 0$ case thanks to the non-zero turbulent heat transport at the crest plane. Some configurations also present an increase in heat flux relative to the baseline smooth wall. In particular, super-hydrophobic longitudinal bars are found to reduce drag and enhance heat flux at the same time. Similarly, the heat transfer efficiency is positively affected for $We \neq 0$.

In conclusion, despite the assumption made in this analysis respect to realistic LIS/SHS, the present results depict a promising scenario for the adoption of these surface treatments in thermal applications. Further studies are still needed to fully characterize turbulent heat transfer over LIS

and SHS and appraise more in depth the dependence of the surface performance to the various parameters at play, including, for instance, sensitivity to the Weber number and fluid properties (viscosity and diffusivity ratios).

REFERENCES

- Arenas, I., García, E., Fu, M. K., Orlandi, P., Hultmark, M. & Leonardi, S. 2019 Comparison between superhydrophobic, liquid infused and rough surfaces: a direct numerical simulation study. *J. Fluid Mech.* **869**, 500–525.
- Daniello, R. J., Waterhouse, N. E. & Rothstein, J. P. 2009 Drag reduction in turbulent flows over superhydrophobic surfaces. *Phys. Fluids* **21** (8), 085103.
- García Cartagena, E. J., Arenas, I., Bernardini, M. & Leonardi, S. 2018 Dependence of the Drag Over Super Hydrophobic and Liquid Infused Surfaces on the Textured Surface and Weber Number. *Flow Turbul. Combust.* **100** (4), 945–960.
- Fu, M. K., Arenas, I., Leonardi, S., Hultmark, M. 2017 Liquid-infused surfaces as a passive method of turbulent drag reduction. *J. Fluid Mech.* **824**, 688–700.
- Fukagata, K., Kasagi, N. & Koumoutsakos, P. 2006 A theoretical prediction of friction drag reduction in turbulent flow by superhydrophobic surfaces. *Phys. Fluids* **18**, 051703.
- Han, J. C., Dutta, S. & Ekkad, S. 2000 *Gas Turbine Heat Transfer and Cooling Technology*. Taylor and Francis.
- Lauga, E. & Stone, H. A. 2003 Effective slip in pressure-driven Stokes flow. *J. Fluid Mech.* **489**, 55–77.
- Leonardi, S., Orlandi, P., Djenidi, L. & Antonia, R. A. 2015 Heat transfer in a turbulent channel flow with square bars or circular rods on one wall *J. Fluid Mech.* **776**, 512–530.
- Martell, M. B., Perot, J. B. & Rothstein, J. P. 2009 Direct numerical simulations of turbulent flows over superhydrophobic surfaces. *J. Fluid Mech.* **620**, 31–41.
- Navier, C. L. M. H. 1823 Mémoire sur les lois du mouvement des fluides. *Mémoires de l'Académie Royale des Sciences de l'Institut de France* **6**, 389–440.
- Orlandi, P. 2000 *Fluid Flow Phenomena. A Numerical Toolkit*. Kluwer Academic.
- Orlandi, P. & Leonardi, S. 2006 DNS of turbulent channel flows with two- and three-dimensional roughness. *J. Turbul.* **7**, N53.
- Orlandi, P. & Leonardi, S. 2008 Direct numerical simulation of three-dimensional turbulent rough channels: parameterization and flow physics. *J. Fluid Mech.* **606**, 399–415.
- Orlandi, P., Leonardi, S. & Antonia, R. A. 2006 Turbulent channel flow with either transverse or longitudinal roughness elements on one wall. *J. Fluid Mech.* **561**, 279–305.
- Park, H., Park, H., Kim, J. 2013 A numerical study of the effects of superhydrophobic surface on skin-friction drag in turbulent channel flow. *Phys. Fluids* **25**, 110815.
- Rastegari, A. & Akhavan, R. 2015 On the mechanism of turbulent drag reduction with super-hydrophobic surfaces. *J. Fluid Mech.* **773**, R4.
- Rosenberg, B. J., Van Buren, T., Fu, M. K. & Smits, A. J. 2016 Turbulent drag reduction over air-and liquid-impregnated surfaces. *Phys. Fluids* **28** (1), 015103.
- Sewall, E. A., Tafti, K. D., Graham, A. B. & Thole, K. A. 2006 Experimental validation of large eddy simulations of flow and heat transfer in a stationary ribbed duct. *Intl. J. Heat Fluid Flow* **27**, 243–258.